JOURNAL OF MATERIALS SCIENCE 20 (1985) 4298–4308

Crystallization kinetics of Mo–N

E. H. HENNINGER
DePauw University, Greencastle, Indiana 46135, USA

D. S. EASTON
Metals and Ceramics Division, Oak Ridge National Laboratory, Oak Ridge, Tennessee 37831, USA

Thin film samples of molybdenum were electron-beam evaporated at 80 K in a 6.6×10^{-4} Pa partial pressure of nitrogen and subsequently analysed for structure, superconductivity and crystallization behaviour. X-ray diffraction of as-deposited samples showed a typical amorphous structure and f c c and b c c phases upon heating. A superconducting transformation at 7.0 to 7.2 K was detected by the resistivity technique. Isothermal DSC scans obtained for a range of temperatures were calibrated and integrated to produce transformed volume (x)–time data. All plots of $\ln[-\ln(1-x)]$ against $\ln t$ have two linear regions with slopes of $n_1 \cong 3.6$ for $0 < x < 0.5$ and $n_2 \cong 2.0$ for $0.7 < x < 1$; where n is the principal parameter in the Johnson–Mehl–Avrami theory of the crystallization transformation. The relationship of this binary pattern of crystallization to the observation of two apparent crystallization peaks in dynamic DSC scans of several samples of electron-beam deposited Mo–N and to the appearance of both Mo-b c c and Mo_2N-f c c phases in the X-ray patterns of the crystallized samples is discussed. Possible patterns of simultaneous or successive modes of nucleation and growth, including combinations of varying nucleation rates, different dimensionals of growth, and interfacial and diffusion controlled growth, are considered.

1. Introduction

Within the field of metallic glasses interest in crystallization behaviour has seen a particularly rapid growth. Because the unique and favourable properties of many glasses are lost or greatly diminished upon irreversible transformation to the stable crystalline state, it is clearly important to know the glass–crystal transformation temperature, T_x. Upon heating, the glass may relax through a series of metastable structures with possible changes in thermodynamic properties [1].

The kinetics of the thermal evolution and the crystallization temperature itself are subject to variation due to composition, sample homogeneity, concentration of nucleation sites, diffusion parameters, and the existence of and possible separation of multiple amorphous phases. These features themselves can vary among samples of the same alloy prepared by different techniques, such as splat quenching, melt spinning and vapour deposition [2]. Finally, the annealing behaviour can depend on the thermal history and the immediate rate of heating of the sample.

An understanding of the processes (relaxation mechanisms, reactions, etc.) active in the glass during annealing and the dependence of this behaviour on sample preparation is important from the practical standpoint, as well as the scientific interest. Such information is significant as well in the search for favourable crystalline microstructures produced by the controlled up-quenching of glasses.

Much work has been reported on crystallization behaviour in Fe–B, Pd–Si, and Cu–Zr alloys [3, 4]. Techniques include measurement of

0022–2461/85 $03.00 + .12

electrical resistivity, magnetic saturation, Mössbauer spectroscopy, and differential scanning calorimetry (DSC). The present work is believed to be the first to examine the crystallization behaviour of molybdenum–nitrogen. An isothermal DSC technique was used.

2. Theory

The accepted model for the crystallization of metallic glasses is the Johnson–Mehl–Avrami equation (JMA) [5–7]. This relation describes three-dimensional random nucleation and growth within an amorphous matrix. It accounts for mutual impingement of growing regions through the concept of "extended volume". Avrami's general relation of the JMA equation states

$$x = 1 - \exp(-bt^n), \quad (1)$$

where x is the volume fraction transformed at time t, n is an exponent which varies from $n = 4$ for a constant nucleation rate to $n = 3$ for a zero nucleation rate (i.e. saturation of point sites) ([8] p. 15), and b is a temperature dependent rate constant. This constant is assumed to reflect Arrhenius behaviour:

$$b = b_0 \exp(-E/RT), \quad (2)$$

where b_0 is a pre-exponential constant, T is absolute temperature, and E is an activation energy for the transformation, i.e. for removal of an atom from the amorphous matrix and migration across the interface on to a crystallite or diffusion to a nucleation site.

From the JMA equation it is seen that the dimensions of b are t^{-n}. The factor b represents a product of nucleation rate and growth rate. More complex analysis shows that the JMA equation can also apply for linear growth with non-random nucleation and for the early stages of diffusion controlled growth. For interface controlled growth, eutectoid reactions, and polymorphic changes, n may be less than 3 if grain edge or grain-boundary nucleation is significant. If an increasing nucleation rate exists (e.g. self-heating effects) n may be greater than 4. Values of $n < 3$ are observed for diffusion controlled growth, reflecting a variety of possible nucleation rates and shapes of growth regions (spheres, plates, needles, etc.) ([8] p. 534).

3. Sample preparation and preliminary characterization

The DSC measurements were made on Mo–N samples originally produced by electron-beam evaporation of pure molybdenum in the presence of a partial pressure of nitrogen gas. The molybdenum and nitrogen atoms were co-deposited on to a cooled (80 K) copper substrate in the form of an amorphous thin film. The film was removed from the substrate at room temperature and analysed for structure and superconductivity.

Although a large series of Mo–N films were deposited in nitrogen pressures ranging from $\sim 2 \times 10^{-4}$ to 12×10^{-4} Pa, the crystallization kinetics reported here concentrated on two films labelled Mo–N–I and Mo–N–II. Both of these films were formed in a nitrogen pressure of 6.6×10^{-4} Pa, but Mo–N–I was deposited while a bias potential of -50 V was applied to a cylindrical electrode located near the substrate and Mo–N–II was deposited with zero bias potential.

X-ray diffraction of samples of these films produced the broad pattern characteristic of an amorphous structure (Fig. 1a). The dominant first peak occurred at $\sin\theta/\lambda$ values of $0.220\,\text{nm}^{-1}$ for Mo–N–I and $0.222\,\text{nm}^{-1}$ for Mo–N–II. Pure molybdenum has a bcc structure with a lattice constant $a = 0.315$ nm. If one uses the above $\sin\theta/\lambda$ values in the Bragg equation and then assumes a (1 1 0) reflecting and calculates the corresponding lattice constant, one finds values of 0.322 and 0.319 nm, respectively. Thus the X-ray results suggest an expansion by the inclusion of nitrogen atoms. Similar lattice expansions are reported in other studies [9, 10].

The films were tested for superconductivity by the resistivity technique. The superconductivity transformation occurred at 7.0 and 7.2 K, respectively, for Mo–N–I and Mo–N–II.

The composition of the films was not determined but is estimated to be ~ 33 and 25 at % nitrogen for Mo–N–I and Mo–N–II, respectively, based on the results of related measurements on the series of Mo–N films noted earlier [11].

4. Calorimetry

Fig. 2 represents the DSC dynamic scans of sample Mo–N–I and a commercial melt-spun $Fe_{40}Ni_{40}P_{14}B_6$ alloy (Ventron $\pm$98646). The

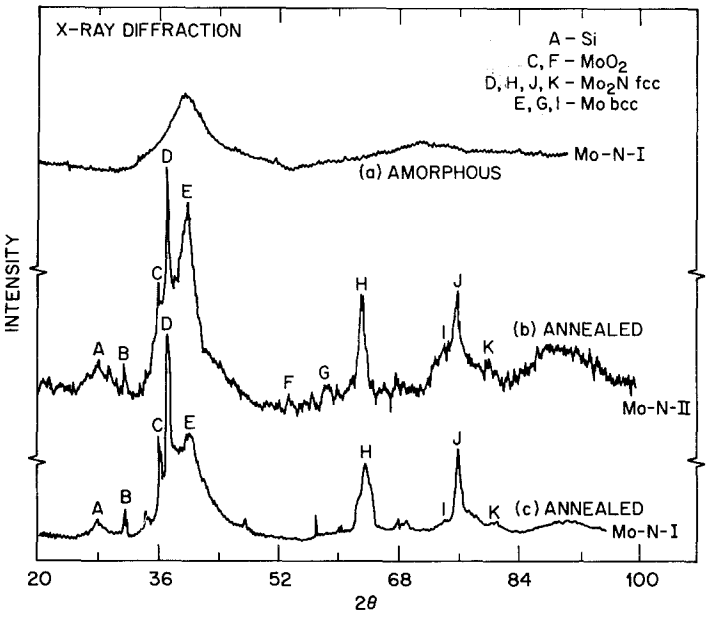

Figure 1 X-ray diffraction patterns; (a) Mo–N–I as-deposited, (b) Mo–N–II after annealing, (c) Mo–N–I after annealing.

latter was measured as a comparison, but its analysis is interesting in its own light.

The areas under the peaks in Fig. 2 yield the enthalpies of the transformation once instrumental calibration factors have been determined. For the purpose of obtaining the crystallization parameters n and b of the JMA equation and the activation energy, one may use several dynamic scans stopped after achieving varying fractions of transformed volume (the Kissinger method [12]), or one may measure the time dependence of the exothermic power at various fixed temperatures near and below T_x.

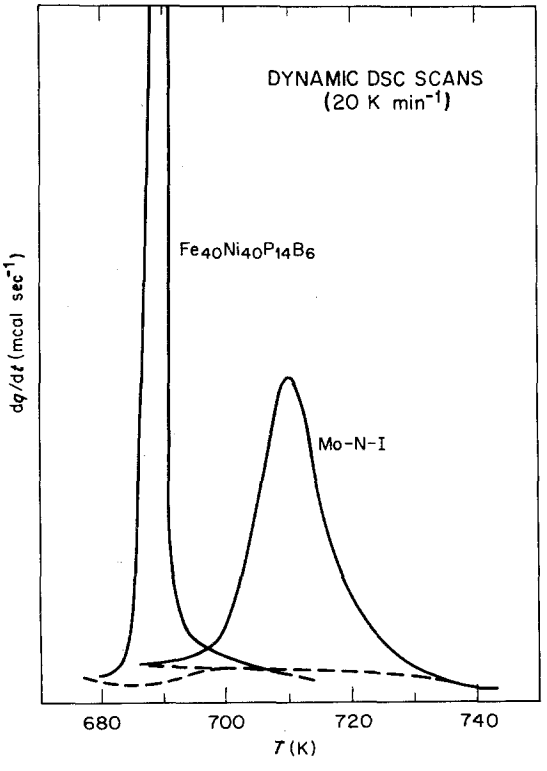

Figure 2 Differential scanning calorimeter results; dynamic method at heating rate of 20 K min^{-1}.

Yinnon and Uhlmann [13] reviewed a large number of mathematical methods to analyse crystallization kinetics based on thermoanalytical studies and concluded that, in general, non-isothermal transformation cannot be treated analytically. Henderson [14] states that the JMA equation is limited in non-isothermal conditions and only applies to crystallization where the growth rate is controlled by temperature and is independent of time. A critical comparison of isothermal with non-isothermal analysis is reviewed by Henderson [15]. These reservations of the non-isothermal technique, together with the fact that the isothermal approach appeared to be simpler, directed the decision to use the latter approach in this work.

Fig. 3 shows the isothermal anneals of samples of Mo–N–I at 665, 670, 675 and 680 K. Sample Mo–N–II also had a dynamic transformation with a peak near 710 K. Isothermal anneals of samples of this film covering the range 680 to 772 K were observed. Because some of these samples were of small mass, and because this temperature range overlaps the dynamic T_x,

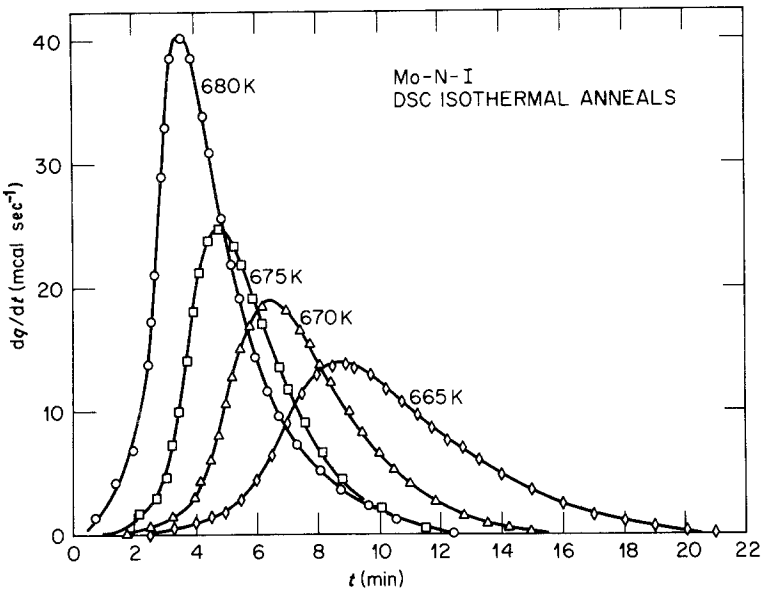

Figure 3 Differential scanning calorimeter results; isothermal method. Mo–N–I, curves normalized to equal mass.

many of the Mo–N–II isothermal anneals had weak peaks and/or overlapped the 15 sec transient time of the DSC. This, in turn, led to difficulty in determining baselines. (Nevertheless, as indicated later in Table I and Figs. 5, 7 and 9, kinetic parameters for this film were obtained.)

In all of the isothermal measurements the sample was heated to 580 K at the slow rate of 40 K min^{-1}. The heating rate was then set to 160 K min^{-1}, and the sample was heated to the test temperature at that rate. The initial slow heating to 580 K allowed time for adjustment of the instrumentation slope and zero set controls as needed to maximize the likelihood that the DSC output would be on scale on the recorder after the transient at the test temperature. The rapid heating stage is often run at a rate of 320 K min^{-1}. The slower 160 rate used here is still rapid enough to prevent significant onset of crystallization during the rise to the temperature, but it may have had the effect of reducing the incubation period [16]. The use of samples with mass greater than 3 mg is desirable, even at the sacrifice of some measurements on limited sample material, in order to gain the instrumentational stability available at lower sensitivity.

5. Data and analysis

The ordinate in both dynamic and isothermal DSC scans is proportional to the net power input to the sample relative to the power input to a stable reference sample. The instantaneous rate of change of the volume fraction of transformed material is

$$\frac{dx}{dt} = \frac{1}{\Delta H}\frac{dq}{dt} \tag{3}$$

where dq/dt is the power, ΔH is the enthalpy of the transformation, and one assumes that the heat per gram of the transformation is uniform in time. ΔH is obtained from the total area between the transformation curve and a properly constructed baseline. Integration of the experimental isothermal DSC curve from $t = 0$ at the start of the transformation to any later time t yields a partial area β, measured in the same units as is the total area α, such that $\beta = \alpha x$, since $x = 1$ at completion. Thus the DSC record yields the volume fraction $x(t)$ as the ratio of the corresponding partial area to the total area β/α. The peak areas were measured with a planimeter. In addition to repeated measurements of successive incremental areas, large overlapping areas were also measured as a check against a possible large error accumulation. Thus even at values of β approaching α the error in x is no more than 3%. Figs. 4 and 5 show the sigmoidal pattern typical of JMA transformations. The increments chosen for calculation of the $x(t)$ values are indicated by the spacing of the points along the time axis.

From the JMA equation one derives

$$\ln[-\ln(1 - x)] = \ln b + n \ln t. \tag{4}$$

If a ln–ln plot of $-\ln(1 - x)$ against t yields a straight line, one can assume that the trans-

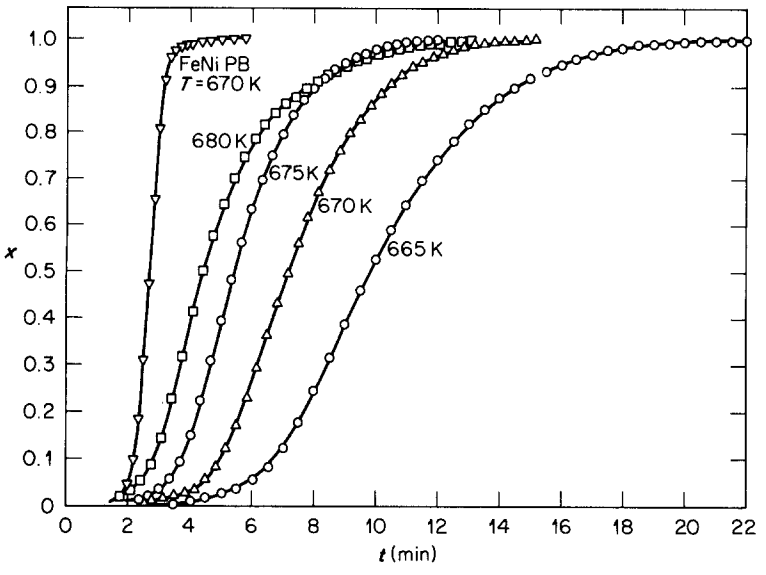

Figure 4 Volume fraction of sample crystallized (X) against time of anneal at temperature T, Mo–N–I and sample $Fe_{40}Ni_{40}P_{14}B_6$.

formation is not inconsistent with the JMA theory of transformations. The parameters n and b can be determined from the slope and intercept, respectively. The values of n and b collected in Table I were determined by linear regression analysis and are consistent with the values obtained directly from the ln–ln plots. Fig. 6 is such a plot for the Ventron alloy.

Adding the assumption of Arrhenius behaviour, in the form $b = b_0 \exp(-E/RT)$, one obtains

$$n \ln t = E/RT + \ln[-\ln(1 - x)] - \ln b_0. \quad (5)$$

The activation energy can be deduced by choosing any specific fraction x_f and reading the corresponding time t_f from the sigmoidal curves obtained at the various temperatures T. A plot of $\ln t_f$ against T^{-1} then yields a straight line with a slope equal to $(E/n)/R$. The activation energy in eV atom^{-1} is calculated as slope $\times$ R, where R is the universal gas constant (8.62×10^{-5} eV atom^{-1} K^{-1}). Activation energies quoted in the literature [16, 17] may vary depending on the author's expression and use of Arrhenius equation. Figs. 7 and 8 show a series of such $\ln t_f$ against T^{-1} plots at fractions $f = 0.15$, 0.50, and 0.85 for Mo–N–II and Mo–N–I respectively.

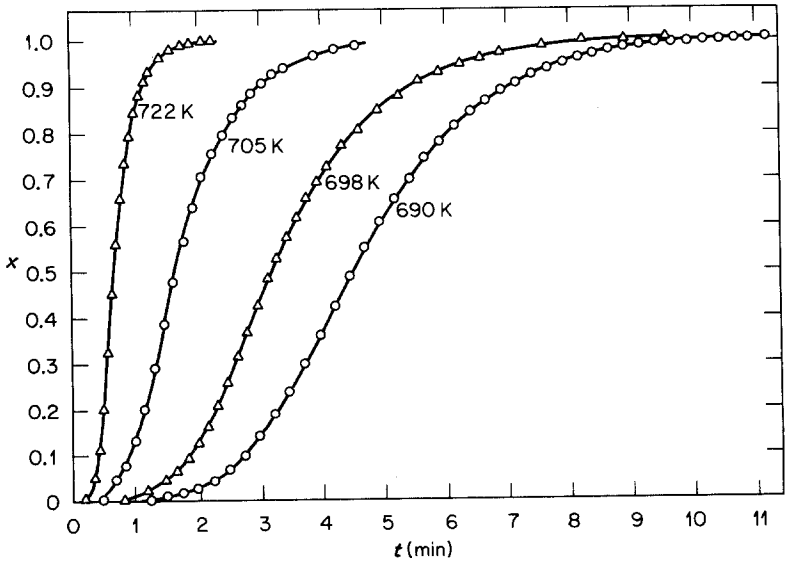

Figure 5 Volume fraction of sample crystallized against time of anneal at temperature T, Mo–N–II.

TABLE I Isothermal anneal data

T (K)	τ (min)	t_f(min) for f = 0.85	0.50	0.15	n_1	Range of x	n_2	Range of x	b_1 (min^{-n})	b_2 (min^{-n})	ΔH ($kJ\,mol^{-1}$)
Sample Mo–N–I, $P = 6.6 \times 10^{-4}$ Pa N_2, Bias = −50 V, T_x = 708 K (sharp)											
680	0.40	6.42	4.00	2.7	3.8	0.06–0.50	1.5	0.78–0.98	0.0047	0.112	7.86
675	1.00	6.49	4.42	3.05	3.9	0.06–0.48	2.2	0.69–0.99	0.0018	0.035	5.97
670	1.00	8.76	6.17	4.35	4.3	0.04–0.50	2.7	0.72–1.00	0.0003	0.006	5.66
665	2.50	10.91	7.33	4.85	3.3	0.04–0.65	2.2	0.65–0.99	0.0010	0.001	9.75
Sample Mo–N–II, $P = 6.6 \times 10^{-4}$ Pa N_2, Bias = 0, T_x = 709 K (broad)											
722	–	0.332	0.72	0.47	3.6	0.01–0.45	1.6	0.84–0.99	2.8	2.0	6.29
715	–	1.97	1.13	0.77	3.4	0.05–0.44	0.7	0.91–1.00	0.40	1.4	10.4
705	–	2.77	1.72	1.03	2.9	0.05–0.64	1.4	0.81–0.99	0.17	0.56	–
698	–	5.10	3.28	2.12	3.6	0.01–0.48	1.85	0.77–1.00	0.013	0.095	9.52
690	–	6.62	4.60	3.07	3.9	0.01–0.36	2.5	0.48–0.98	0.0016	0.019	7.21
Sample $Fe_{40}Ni_{40}P_{14}B_6$, T_x = 688 K											
672	1.14	1.38	1.08	0.74	4.3	0.12–1.00			0.52		4.68
670	1.33	1.72	1.35	0.95	4.0	< 0.01–0.96			0.135		

6. Results

Figs. 3 to 5 exhibit crystallization kinetics typical of metallic glasses. The sigmoidal Mo–N curves of Figs. 4 and 5 do, however, approach the $x = 1$ limit much less sharply than does the FeNiPB sample. The plots of Figs. 6, 9 and 10 show that the behaviour in the Mo–N samples is more complex. The single straight line fit of the FeNiPB data to the JMA equation (up to $x = 0.96$, beyond which the $\ln[-\ln(1-x)]$ varies rapidly) is clearly contrasted to the double-slope-with-transition region behaviour of the Mo–N samples.

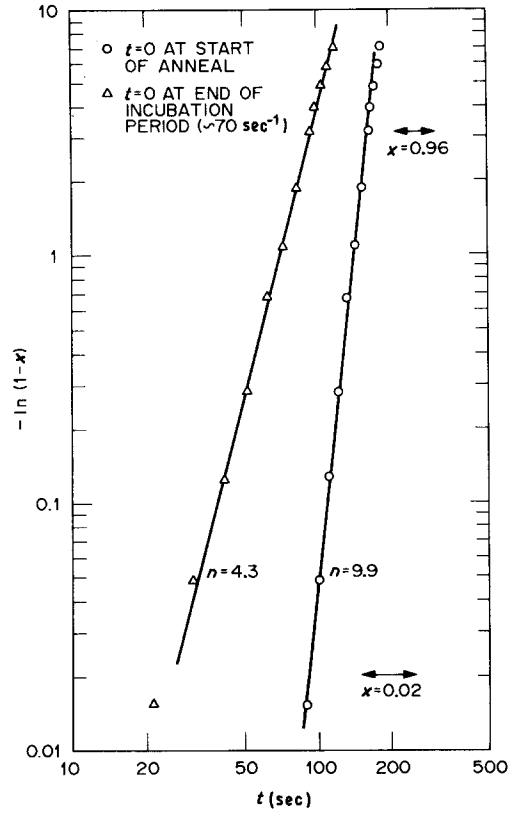

Figure 6 $-\ln(1-x)$ against time of anneal, showing effect of incubation time on calculated value of n; sample $Fe_{40}Ni_{40}P_{14}B_6$ at 627 K.

Table I summarizes the parameters. The transformation temperatures T_x listed here represent the temperatures at which the rate of transformation is greatest for a 20 K min^{-1} rate of annealing. T_x is usually taken to be the temperature at the onset of the transformation and this is a significantly lower value for the Mo–N sample (see Fig. 2) due to the broad nature of the peak. The observed incubation time (τ) at the annealing temperature is related to the time for quenched-in nuclei to transform into effective structures for growth. Clearly this depends on the annealing temperature. For Mo–N–II the annealing temperatures chosen overlapped T_x so that in all but one sample τ is at least less than the 15 sec instrument transient. The dq/dt data were obtained by subtracting a baseline from the experimental curve. A lever rule calculation was used for the baseline determination (see baselines in Fig. 2) but some intuitive modification was required for those curves whose leading baseline was lost in the transient. The 85, 50 and 15% transformed times (t_f) were read from the sigmoidal curves (x against t). All times listed

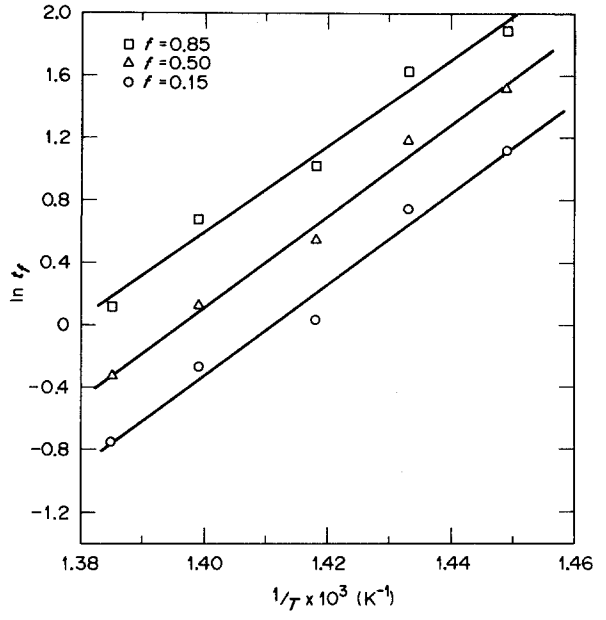

Figure 7 ln (time to fraction f crystallized) against T^{-1}; Mo–N–II. Activation energy = slope × R = 2.6 eV.

in Table I and plotted in Figs. 7 and 8 refer to $t = 0$ at the end of the incubation period. The slopes n_1 for the early straight line behaviour, and n_2 for the late straight line behaviour, were determined directly from the graphs and by linear regression analysis of the x–t data in the ranges of x indicated in Table I. The linear regression values of n_1 and n_2 are shown in Table I.

The rate constants b can be calculated as averages of values calculated from the JMA equation using the n value and various x, t pairs on the line. However, the b values in Table I were produced automatically by the linear regression programme. The correlation coefficients, r, were of the order of 0.996 for all straight line fits in Figs. 6, 9 and 10 and Table I. This is reassuring since it is evident from the ln–ln plots that a slight variation in the drawing of the line represents a large change in slope n.

Figs. 7 and 8 follow from the data of Table I.

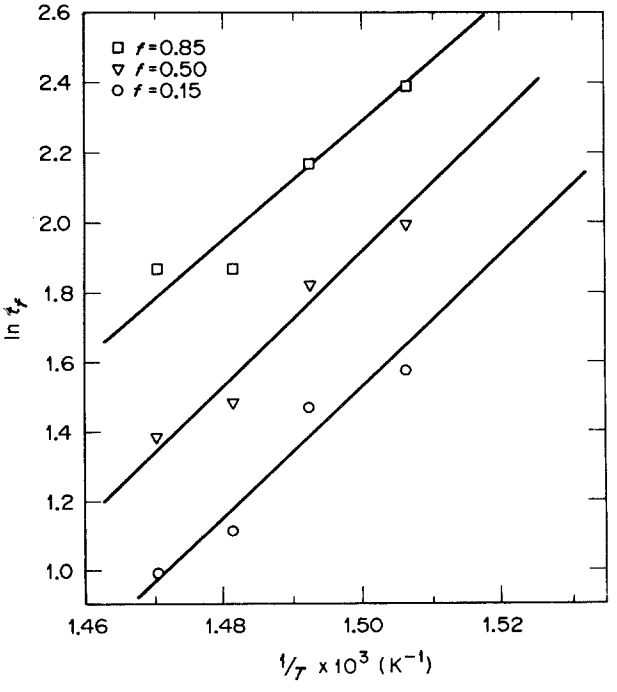

Figure 8 ln (time to fraction f crystallized) against T^{-1}; Mo–N–I. Activation energy = slope × R = 1.7 eV.

TABLE II

Sample	$\bar{n}_{\parallel}$†	x^*‡	ΔH (kJ mol^{-1})	E/n (eV)§	Crystal phases present
Mo–N–I	3.8 ± 0.5	0.53 ± 0.06	7.3 ± 2.3	1.7	fcc – Mo_2N + trace of bcc-Mo
Mo–N–II	3.5 ± 0.4	0.47 ± 0.09	8.3 ± 2	2.6	fcc – Mo_2N + significant bcc-Mo
$Fe_{40}Ni_{40}P_{14}B_6$	4.0, 4.3 (3.5–4.4)		4.68	(4.0)¶	

†n is the slope of $-\ln(1-x)$ against τ for values of $x < x^*$.
‡x^* is the volume fraction value at which the slope changes from n_1 to n_2.
§E/n is the activation energy.
¶Scott and Ramachandraro [16].

Reasonable straight line fits ($r > 0.98$) seem to justify the Arrhenius relation, and the slopes of the lines were then used to calculate activation energies. Average values are summarized in Table II.

Average values for n_1 are presented in Table II for each of the samples. The spread of values of n_1 for each sample suggests an alternative analysis. The b_1 values from Table I for Mo–N–II are plotted as ln b_1 against T^{-1} in Fig. 11. A straight line fit, as required for the Arrhenius relation, is reasonably well achieved. If the 705 K point is adjusted to fit this line and the adjusted b_1 value used in Equation 5 with $t = t_{0.50}$ to calculate n_1, a result of 3.9 follows. This contrasts with the

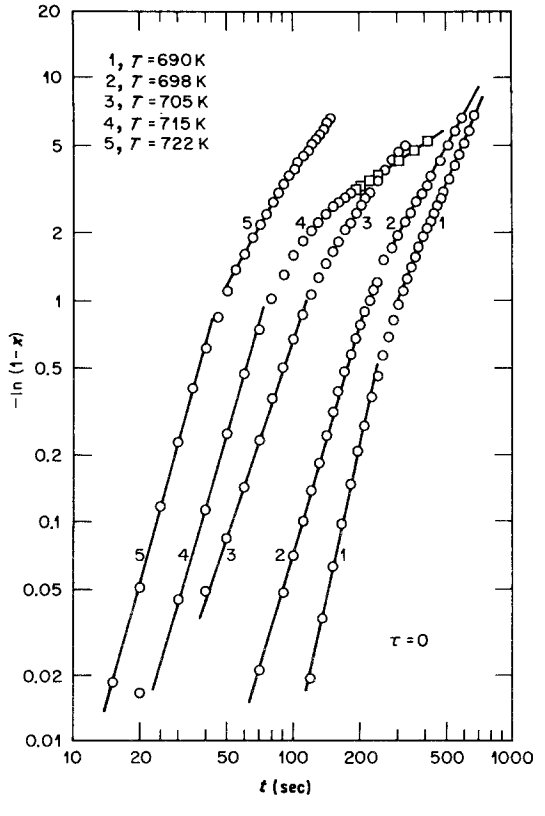

Figure 9 –ln (1 – x) against time of anneal; Mo–N–II.

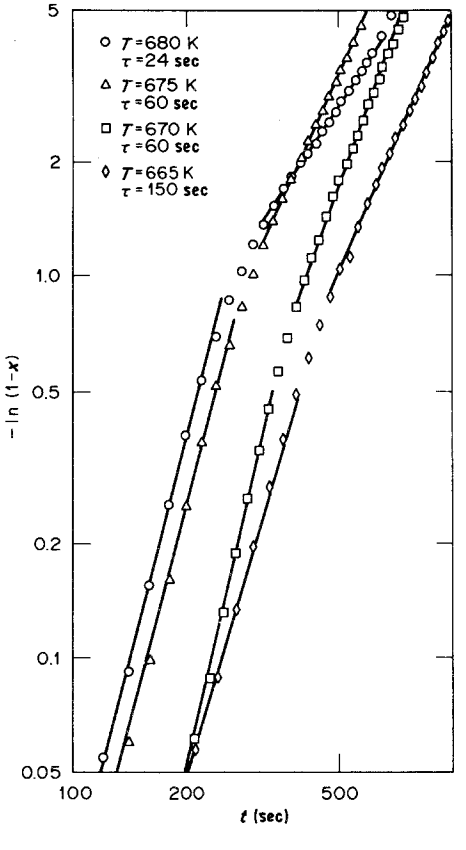

Figure 10 –ln (1 – x) against time of anneal; Mo–N–I.

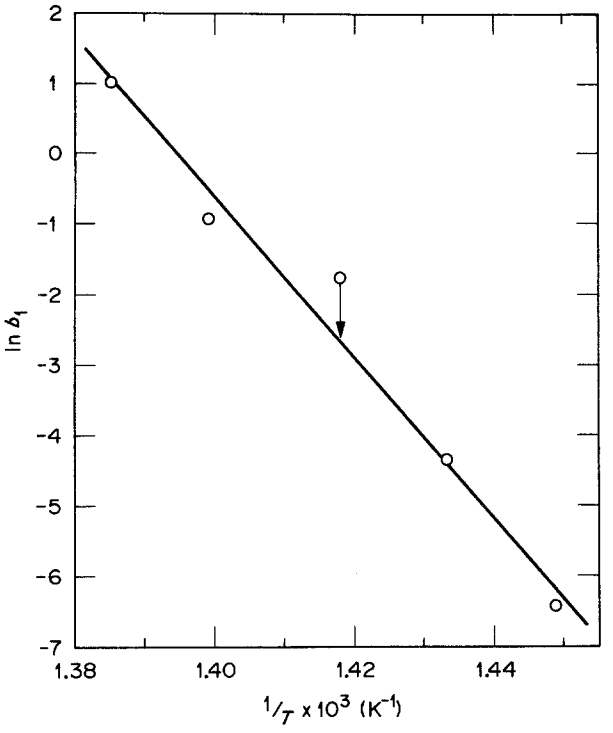

Figure 11 ln b_1 against T^{-1}, Mo–N–II.

original $n_1 = 2.9$ and is closer to the average value of 3.8. Similarly, using the (Mo–N–I) data, adjustments of the 670 and 665 K values to 3.8 and 4.2 are suggested. The slopes of these lines represent, on the Arrhenius model, the activation energy. Using $n = 3.8$ and 3.5, respectively, the slopes yield $E/n = 2.1$ and 2.8 eV for Mo–N–I and Mo–N–II, respectively, compared to 1.7 and 2.6 from Table I, via plots of Equation 5.

This "back door" analysis for n and E/n is probably of supplementary value only since the adjusted n values calculated vary with choice of x and t_x used in Equation 5. This reflects a need for an accurate determination of the time of onset of the crystallization. Such an analysis for n_2 values via the b_2 data in Table I was of no use, no doubt because any choice of t_x has no correlation with the onset of n_2 kinetics (if it even is an independent crystallization event).

The heats of transformation, ΔH, were measured from the areas under the isothermal dq/dt against t curves [11].

7. Discussion

7.1. $Fe_{40}Ni_{40}P_{14}B_6$

Fig. 6, though not of direct significance to the Mo–N, is of interest because of its clear illustration of Scott and Ramachandraro's argument [16] *vis á vis* their results and Coleman's early published results for this alloy [18]. As in Coleman's paper, we find here that an extraordinarily large n value, beyond that explicable by an accepted nucleation and growth model, is obtained if the incubation time is not accounted for. The properly obtained n values agree with Scott's result (Table II). The plot obtained with a shifted time scale is still a straight line, and thus, fits the JMA theory i.e. the equation $1 - x = \exp[-b^1(t + s\,\tau)^{n^1}] = \exp[-bt^n]$. However, this is rather deceptive since a ln t curve can be very closely aligned with a ln $(t + \tau)$ curve by raising the one by an additive constant (essentially b^1) and twisting the other by a multiplicative constant (n). Thus, meaningful values of n, b, and activation energy require correct determination of the time of the start of the transformation, and this requires an experimental technique in which a good leading baseline is obtained.

7.2. Mo–N

The double slope of the Mo–N crystallization curves (Figs. 9 and 10) recalls the binary character of both the X-ray diffraction results and the dynamic crystallization curves. In the latter, a double peak was observed in the series studied by Easton *et al.* with a higher temperature T_{x2}

associated with crystallization of a fcc Mo_2N phase [11]. The X-ray patterns (Fig. 1) indeed exhibit the presence of both crystalline structures after complete annealing. The Mo_2N phase is dominant in both samples, more so in Mo–N–I. There is a suggestion that bias voltage enhanced nitrogen incorporation in the Easton *et al.* study [11].

In that study, it was determined that at nitrogen pressures $\geqq 6.6 \times 10^{-4}$ Pa the fcc phase dominated and the T_{x1} peak was not discernible, hence, the dynamic curve of Fig. 2 does not appear to have a double peak despite the crystallization of both phases. The curve is, however, broader and less abrupt at the low temperature shoulder than would be expected for a simple transformation.

The question then is "Are the n_1 and n_2 crystallization kinetic parameters representative of formation of bcc Mo and fcc Mo_2N phases, respectively, with the bcc crystallization occurring first or at least dominant energetically in the early stages, or do the n_1 and n_2 parameters relate to different modes of crystallization regardless of whether one phase or the other or both may be forming?"

It may be helpful to examine the Mo–N results in the light of the approximate model

$$n = a + bp, \tag{6}$$

where a accounts for the nucleation rate and varies from zero (for quenched-in nuclei) to 1 (for a constant uncleation rate), b defines the dimensionality of the growth ($b = 1$, 2, or 3), p has the value 1 for interfacial control of growth (assumed linear in time), and $p = 0.5$ for diffusion controlled growth [4].

Thus, the average n_1 values of 3.8 and 3.6 for Mo–N–I and Mo–N–II point to three-dimensional interfacial controlled growth with a nearly constant nucleation rate. The n_2 values of the order of 1.5 to 2.7 for Mo–N–I and 0.7 to 2.5 for Mo–N–II suggest possibilities of (1) site saturation ($a = 0$) with grain-boundary growth ($b = 2, p = 1$), so that n = 2; (2) site saturation ($a = 0$) with grain edge growth ($b = 1, p = 1$), so that $n = 1$; (3) constant nucleation rate ($a = 1$) with grain edge growth ($b = 1, p = 1$) so that $n = 2$; (4) three-dimensional diffusion controlled growth ($t = 3, p = 0.5$) with zero to constant nucleation rate ($a = 0$ to $a = 1$), so that n ranges from 1.5 to 2.5.

Finally, one may compare the results here to the discussion of Section 57 of Christian [8]. Christian shows that the JMA kinetics can apply in some cases of grain-boundary nucleation, and that a shift in slope from $n = 4$ to $n = 1$ occurs with a bend observed between the linear segments. The change in slope is interpreted as a saturation of grain-boundary nucleation sites, "before saturation occurs, the fact that nuclei are confined to grain boundaries scarcely affects the overall volume fraction transformed". After site saturation, growth becomes the factor ruling the kinetics (and the value of n).

Furthermore, Christian states that even if this experimental effect exists, it will be observed only if the bend occurs when the volume fraction, x, is about 0.5. This $x \cong 0.5$ value at the bend seems well obeyed in the Mo–N plots as summarized in the x-range values of Table I. The inclination to attribute the Mo–N kinetics to grain-boundary nucleation is dampened somewhat by Christian's further observation that the highly temperature-dependent character of the nucleation rate makes it unlikely that the bend would be observed over a significant temperature range. The bend is observed in all of the Mo–N plots covering a large temperature range.

The particular nucleation and growth kinetics active in the Mo–N crystallization cannot be unequivocally specified from analysis of these data. There is good reason to believe that bcc Mo starts crystallizing with a nearly constant nucleation rate and an interface controlled three-dimensional growth linear in time. The latter part of the crystallization event is dominated by, or it at least includes, fcc Mo_2N crystallization, possibly by diffusion of nitrogen to pre-existing Mo_2N nuclei. The presence, after annealing, of Mo_2N in samples representing a wide range of nitrogen pressures, in contrast to the narrow composition range predicted for fcc Mo_2N, supports the supposition of pre-existent Mo_2N nuclei.

The possibility in a real transformation of the presence of several kinds of sites (random volume, grain-boundary, grain edge, etc.) with different nucleation rates and different modes of growth makes it extremely difficult to interpret the experimental crystallization kinetics, even if only a single phase is involved. It might be mentioned that an attempt to synthesize the dq/dt–t curve as a superposition of two simultaneous

JMA events, i.e. $x = 1 - \exp(-b_1 t^{n_1}) - \exp(-b_2 t^{n_2})$, did not come close.

The activation energies obtained from Figs. 7 and 8 and reported in Table II are in line with those reported for other transition metal–metalloid glasses and are lower than those for glasses containing more species (compare the $Fe_{40}Ni_{40}P_{14}B_6$ value in Table II). The fact that the slope of the ln t_f against T^{-1} line for the 85% crystallized time is the same as in the 15 and 50% cases suggests that either the data analysis measures a single activation energy for the event as a whole or that separate activation energies for Mo and Mo_2N crystallization are very nearly equal. The higher activation energy for Mo–N–II may be due to a retarding effect from the presence of more bcc Mo [19].

8. Conclusions

Amorphous thin film samples of Mo–N were produced by electron-beam deposition of molybdenum in a nitrogen atmosphere. The kinetics of the isothermal crystallization of the samples agree with the JMA theory in two distinct stages ($n = 4$ for zero to 50% crystallization, $n = 1.5$ to 2.5 at higher volume fraction crystallization). Activation energies of 2.6 and 1.7 eV were calculated for the two films tested.

The analysis is consistent with a model of constant nucleation rate crystallization and three-dimensional interface controlled growth of bcc Mo followed by diffusion controlled growth of fcc Mo_2N on pre-existing nuclei. However, because of the variety of possible nucleation rates, dimensionalities, and growth mechanisms, it is impossible to clearly identify either successive or simultaneous kinetics of the crystallization of the Mo and Mo_2N phase or their unique or mixed activation energies.

Acknowledgements

The authors wish to thank C. G. McKamey and D. M. Kroeger for their help in discussions and critique of this work. Appreciation is also expressed to Gwendolyn Sims for preparation of this manuscript. This research was sponsored by the Division of Materials Sciences, US Department of Energy under contract DE-AC05-840R21400 with the Martin Marietta Energy Systems, Inc. The US Government retains a nonexclusive, royalty-free license to publish or reproduce the published form of this contribution, for US Government purposes.

References

1. H. S. CHEN, *Rep. Prog. Phys.* **43** (1980) 380.
2. *Idem, ibid.* **43** (1980) 362.
3. U. KOSTER and U. HEROLD, Crystallization of Metallic Glasses, in "Topics in Applied Physics", Vol. 46, edited by H. J. Güntherodt and H. Beck, (Springer-Verlag, New York, 1981).
4. V. R. V. RAMANAN and G. FISH, *J. Appl. Phys.* **53** (1982) 2273.
5. M. AVRAMI, *J. Chem. Phys.* **7** (1939) 1103.
6. *Idem, ibid.* **8** (1940) 212.
7. *Idem, ibid.* **9** (1941) 177.
8. J. W. CHRISTIAN, "The Theory of Transformations in Metals and Alloys", 2nd Edn. (Pergamon Press, London, 1975).
9. P. H. SCHMIDT, *J. Vac. Sci. Technol.* **10** (1973) 613.
10. B. SCHRODER, W. L. JOHNSON, C. C. TSUEI, P. CHAUDHARI and J. F. GRACZYK, *Proc. Int. AIP Conf.* **31** (1976) 353.
11. D. S. EASTON, E. H. HENNINGER, O. B. CAVIN and C. C. KOCH, *J. Mater. Sci.* **18** (1983) 2126.
12. H. E. KISSINGER, *Anal. Chem.* **29** (1957) 1702.
13. H. YINNON and D. R. UHLMANN, *J. Non-Cryst. Solids* **54** (1983) 253.
14. D. W. HENDERSON, *ibid.* **30** (1979) 301.
15. *Idem, J. Thermal Analysis* **15** (1979) 325.
16. M. G. SCOTT and P. RAMACHANDRARO, *Mater. Sci. Eng.* **29** (1977) 137.
17. J. A. LEAKE and A. L. GREER, *J. Non-Cryst. Solids* **38, 39** (1980) 735.
18. E. COLEMAN, *Mater. Sci. Eng.* **23** (1976) 161.
19. V. R. V. RAMANAN, private communication (1983).

Received 30 October
and accepted 28 November 1984